Archives of Civil and Mechanical Engineering (2022) 22:14
https://doi.org/10.1007/s43452-021-00330-3

ORIGINAL ARTICLE

Analytical and parametric analysis of thermoelastic damping in circular cylindrical nanoshells by capturing small-scale effect on both structure and heat conduction

Ming Li[1,2] · Youjie Cai[1] · Li Bao[1,2] · Rui Fan[1] · Hongbin Zhang[1,2] · Hongyan Wang[1] · Vahid Borjalilou[3]

Received: 31 May 2021 / Revised: 24 September 2021 / Accepted: 30 September 2021 / Published online: 26 November 2021

Abstract
This article intends to examine thermoelastic damping (TED) in circular cylindrical nanoshells by considering small-scale effect on both structural and thermal areas. To fulfill this aim, governing equations are extracted with the aid of nonlocal elasticity theory and dual-phase-lag (DPL) heat conduction model. Circular cylindrical shell is also modeled on the basis of Donnell–Mushtari–Vlasov (DMV) equations for thin shells. By inserting asymmetric simple harmonic oscillations of nanoshell into motion, compatibility and heat conduction equations, the size-dependent thermoelastic frequency equation is obtained. By solving this equation and deriving the frequency of nanoshell affected by thermoelastic coupling, the value of TED can be calculated through complex frequency approach. Results of this investigation are given in two sections. First, to appraise the validity of presented formulation, a comparison study is conducted between the results of this work in special cases and those reported in the literature. Next, by providing several numerical data, a detailed parametric study is performed to highlight the profound impact of nonlocality and dual-phase-lagging on TED value in simply supported cylindrical nanoshells. The influence of some determining factors such as mode number and type of material on TED is also evaluated.

Keywords Thermoelastic damping · Cylindrical nanoshell · Size effect · Nonlocal elasticity theory · Dual-phase-lag heat conduction model · Closed-form solution

✉ Rui Fan
rfan02@syr.edu

Ming Li
liming2814324604@163.com

Youjie Cai
fzmjldx@163.com

Li Bao
sherifeig01@hotmail.com

Hongbin Zhang
tieqund@163.com

Hongyan Wang
hongyanweco@yeah.net

Vahid Borjalilou
vahid.borjali@alum.sharif.edu

[1] Mechanical and Electrical Engineering Department, Qiqihar University, Qiqihar 161006, Heilongjiang, China

[2] Collaborative Innovation Center of Intelligent Manufacturing Equipment Industrialization of Heilongjiang Province, Qiqihar 161006, Heilongjiang, China

[3] Department of Mechanical Engineering, Sharif University of Technology, Tehran, Iran

1 Introduction

Given their extraordinary attributes and huge area of applications, small-scaled structural elements such as circular cylindrical nanoshells have received widespread attentions. According to several experimental data, it has been made clear that the size-dependency phenomenon has a conspicuous influence on the static and dynamic behavior of miniaturized structures, which are extensively exploited in micro- and nanoelectromechanical systems (MEMS and NEMS). For instance, by conducting a micro-torsion test on thin copper wires, Fleck et al. [1] indicated that torsional hardening of wire is three times what the theoretical method predicts. Via a micro-indentation experiment, Ma et al. [2] realized that the measured indentation hardness of silver single crystal is more than that estimated by classical formulation. In the micro-bending test on polypropylene microbeams by McFarland et al. [3], it was revealed that the measured stiffness values are at least four times larger than the classical beam theory stiffness predictions. Since classical theory (CT) of continuum pays no heed to submicron

discontinuities in bodies, it is unable to acceptably explicate the size-dependent behavior of mechanical structures with small scales. In consequence, for the sake of incorporating size effect into constitutive relations, size-dependent continuum theories like couple stress theory [4], nonlocal theory (NT) [5], modified couple stress theory (MCST) [6] and strain gradient theory (SGT) [7] have been advanced. As one of these nonclassical theories, nonlocal elasticity theory is based on this hypothesis that the stress at an arbitrary point is pertinent to the strains at all points of the continuum.

The heat transfer process in solid continua has been mathematically expounded through various heat conduction models. On the basis of empirical evidences, the Fourier law on which classical thermoelasticity (CTE) theory has been established cannot satisfactorily interpret heat transfers occurring in very small times or dimensions [8]. On that account, by employing one or more scale parameters, several non-Fourier heat conduction models have been propounded and developed to remove the limitations of Fourier law. By incorporation of a single phase lag parameter into conventional model, Lord and Shulman [9] put forward a model (LS model) including small-scale effect only in time. By attaching an additional phase lag parameter to LS model, Tzou [10] proposed the dual-phase-lag (DPL) model that is capable of capturing small-scale effect in both time and space domains. By description of heat transfer process according to phonon scattering model and solving the linearized phonon Boltzmann transport equation, Guyer and Krumhansl [11] arrived at a robust formulation (GK model) to reflect both nonlocal and lagging characteristics of heat propagation at nano dimensions.

Findings of theoretical and experimental researches signify that thermoelastic damping (TED) is one of predominant intrinsic energy dissipation mechanisms in small-sized structures. This phenomenon emanates from irreversible heat flow induced in the thickness direction of vibrating structures. Due to these transverse irreversible heat currents, strain energy cannot be totally retrieved, which narrows the quality factor of small-scaled mechanical devices. In the following, the most prominent studies conducted on TED in micro- and nanostructures are brought up. The investigation of Zener [12] on TED in thin beams is the first analytical study about TED in structural elements. In this work, an analytical solution in the form of infinite series has been presented to determine the magnitude of TED in Euler–Bernoulli beams. By solving the frequency equation of CTE, Lifshitz and Roukes [13] attained an explicit formula for estimation of TED in Euler–Bernoulli beams with the aid of complex frequency approach. In the work of Lu et al. [14], on the basis of DMV equations for thin shells, an analytical study in the framework of classical continuum theory and heat conduction model has been performed to survey TED in small-scaled cylindrical shells. In an analogous study, Kim and Kim [15] addressed the role of initial stress in the amount of TED in cylindrical shells. Li et al. [16] established an analytical model to specify TED in classical circular and rectangular microplates in the context of energy dissipation approach. Yue et al. [17] evaluated small-scale effect on thermoelastic vibrations of Timoshenko nanobeams according to nonlocal strain gradient theory (NSGT) and GK model. To ascertain size effect on TED in circular nanoplates, by making use of nonlocal theory and DPL model, Xiao et al. [18] extracted an explicit size-dependent expression for TED. Li and Esmaeili [19] exploited nonlocal elasticity theory and GK model to provide a model describing TED in axisymmetric vibrations of circular nanoplates. In the article of Zhong et al. [20], MCST and classical model of heat conduction have been utilized to find an analytical relation estimating TED in Kirchhoff rectangular microplates. Zhang et al. [21] employed MCST and GK model to highlight the influence of scale parameters on TED in small-sized beams. Zhang et al. [22] provided an analytical model to appraise the damping vibrations of plates reinforced with graphene oxide powders in thermal environments. In the context of entropy generation approach, Parayil et al. [23] assessed TED in classical Timoshenko beams with mid-plane nonlinearity. By means of nonlocal strain gradient theory (NSGT) and GK model, Deng et al. [24] developed a theoretical model to appraise size effect on TED in graphene nanobeams. Rashahmadi and Meguid [25] implemented the Galerkin method to predict the magnitude of TED in orthotropic graphene nanosheets using nonlocal elasticity theory. Li and Ma [26] analyzed TED in functionally graded (FG) rectangular microplates with different boundary conditions via classical continuum theory and heat conduction model. With the help of MCST and three-phase-lag (TPL) model, Kumar and Mukhopadhyay [27] achieved a size-dependent solution for TED in thin microplates. With the aim of clarifying small-scale effect on TED in thin rectangular nanoplates, an analytical research has been carried out by Yang et al. [28] on the basis of nonlocal theory and DPL model. By incorporating nonlocal effect within constitutive and heat conduction relations, Ahmadi et al. [29] determined size-dependent value of TED in orthotropic nanoplates. By inclusion of surface and dual-phase-lagging effect into governing equations, Shi et al. [30] derived an explicit solution for TED in nanobeams. Zhou and Li [31] investigated TED in small-sized rectangular and circular plates according to MCST and nonlocal version of DPL model. Paper of Ge et al. [32] has been devoted to determination of size effect on the amount of TED in rectangular plates by utilizing NSGT and GK model. Weng et al. [33] presented a closed-form solution for coupled thermoelastic response of Timoshenko nanobeams by applying NSGT and DPL model. Zhou and Li [34] conducted a theoretical study to illuminate the impact of DPL model on TED in miniaturized rings with rectangular cross

section. With the help of MCST, Arshid et al. [35] surveyed size-dependent vibrations of FG porous sandwich curved microbeams in thermal environments.

Given experimental and theoretical findings mentioned above, utilization of size-dependent continuum theories and heat conduction models in governing equations of small-sized structures leads to more confident predictions about their thermoelastic behavior. Assessment of small-scale effect on TED in circular cylindrical nanoshells in the framework of nonlocal elasticity theory and dual-phase-lag (DPL) heat conduction model is carried out in this paper for the first time. By exploiting Donnell–Mushtari–Vlasov (DMV) model of thin shells, size-dependent coupled thermoelastic equations are established. Next, asymmetric time-harmonic vibrations are adopted to extract the frequency equation affected by thermoelastic coupling. Subsequently, an analytical expression consisting of structural and thermal scale parameters is derived to specify the magnitude of TED in cylindrical nanoshells with arbitrary boundary conditions. With the purpose of evaluating the validity of present formulation, a comparison study is done between the results predicted by this model with those existing in the literature. A complete parametric study is also conducted on simply supported cylindrical nanoshells to focus on the impact of nonlocality, dual-phase-lagging and material on the amount of TED in some vibration modes.

2 Basic theoretical principles

2.1 Fundamentals of nonlocal elasticity theory

Based on the differential form of Eringen's nonlocal elasticity theory [5], the nonlocal stress tensor $\boldsymbol{\sigma}$ and the classical (local) stress tensor $\boldsymbol{t}$ are related to each other via the following relation:

$$\left(1-\mu\nabla^2\right)\boldsymbol{\sigma}=\boldsymbol{t}, \tag{1}$$

in which parameter μ is known as nonlocal parameter. Moreover, symbol ∇^2 represents the Laplace operator. According to coupled thermoelastic constitutive relations of conventional stress tensor $\boldsymbol{t}$, Eq. (1) becomes:

$$\left(1-\mu\nabla^2\right)\boldsymbol{\sigma}=\frac{E}{(1+\nu)(1-2\nu)}\left[\nu\varepsilon_{mm}\boldsymbol{I}+(1-2\nu)\boldsymbol{\varepsilon}-(1+\nu)\alpha\vartheta\boldsymbol{I}\right], \tag{2}$$

where ε_{mm} indicates trace of strain tensor $\boldsymbol{\varepsilon}$. Material properties E and ν are also elasticity modulus and the Poisson ratio. In addition, parameter α stands for the thermal expansion coefficient. Variable $\vartheta=T-T_0$ denotes the temperature increment with T and T_0 as the instantaneous and reference temperatures, respectively. Note that when the nonlocal parameter μ is set to zero, constitutive relations of nonlocal theory reduce to those of classical theory.

2.2 Fundamentals of dual-phase-lag (DPL) heat conduction model

According to DPL heat conduction model for isotropic materials, heat conduction process is formulated through the following relation [10]:

$$\boldsymbol{q}+\tau_q\frac{\partial\boldsymbol{q}}{\partial t}=-k\boldsymbol{\nabla}\vartheta-k\tau_T\frac{\partial\boldsymbol{\nabla}\vartheta}{\partial t}, \tag{3}$$

where $\boldsymbol{q}$ defines the heat flux vector. Furthermore, Material constant k refers to thermal conductivity. Parameters τ_q and τ_T are also called phase lag of heat flux and phase lag of temperature gradient that make it possible to capture small-scale effect in time and space domains, respectively. It is worth mentioning that in the absence of τ_T, the constitutive relation of DPL model corresponds to that of LS model. Additionally, by dropping the terms comprising phase lags τ_q and τ_T, Eq. (3) is reduced to constitutive relation of the Fourier law. The equation of conservation of energy for an isotropic material is expressed by [10]:

$$-\boldsymbol{\nabla}\cdot\boldsymbol{q}=\rho c_v\frac{\partial\vartheta}{\partial t}+T_0\beta\frac{\partial\varepsilon_{mm}}{\partial t}, \tag{4}$$

with ρ and c_v standing for mass density and specific heat per unit mass, respectively. Parameter $\beta=E\alpha/(1-2\nu)$ is also known as thermal modulus. If heat flux $\boldsymbol{q}$ is eliminated from Eqs. (3) and (4), equation of heat conduction in terms of temperature alteration ϑ and cubical dilatation ε_{mm} is derived as below:

$$k\left(1+\tau_T\frac{\partial}{\partial t}\right)\overline{\nabla}^2\vartheta=\left(1+\tau_q\frac{\partial}{\partial t}\right)\left(\rho c_v\frac{\partial\vartheta}{\partial t}+T_0\beta\frac{\partial\varepsilon_{mm}}{\partial t}\right), \tag{5}$$

in which symbol $\overline{\nabla}^2$ defines three-dimensional Laplace operator.

3 Thermoelastic model of cylindrical shells according to nonlocal theory and DPL model

3.1 Motion equations

Figure 1 illustrates the schematic view and geometry of a circular cylindrical shell with length L, radius R and uniform thickness h. On the basis of Donnell–Mushtari–Vlasov (DMV) model of thin shells, the components of displacement field have the following form [36]:

$$u_x=u(x,\theta,t)-z\frac{\partial w(x,\theta,t)}{\partial x},\quad u_\theta=v(x,\theta,t)-\frac{z}{R}\frac{\partial w(x,\theta,t)}{\partial\theta},\quad u_z=w(x,\theta,t) \tag{6}$$

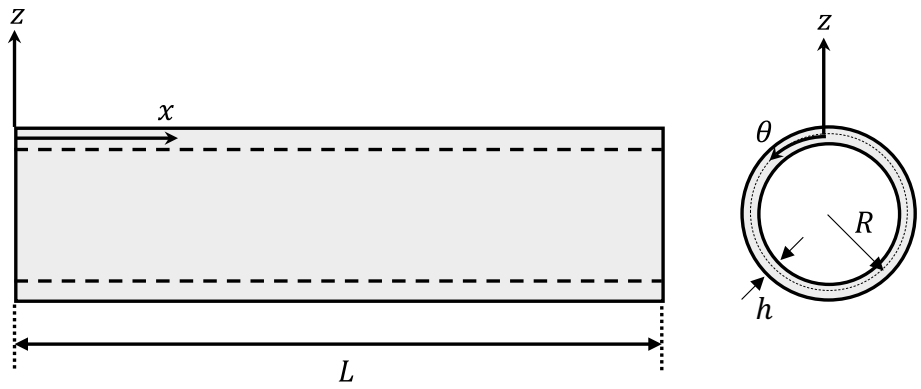

Fig. 1 Schematic view of a circular cylindrical shell

in which u_x, u_θ and u_z refer to the displacements along x, θ and z directions, respectively. By referring to equations above, the nonzero components of strain tensor are expressed by [36]:

$$\varepsilon_{xx} = \varepsilon^0_{xx} + z\kappa_{xx} = \frac{\partial u}{\partial x} - z\frac{\partial^2 w}{\partial x^2}, \tag{7a}$$

$$\varepsilon_{\theta\theta} = \varepsilon^0_{\theta\theta} + z\kappa_{\theta\theta} = \left(\frac{1}{R}\frac{\partial v}{\partial \theta} + \frac{w}{R}\right) - z\left(\frac{1}{R^2}\frac{\partial^2 w}{\partial \theta^2}\right), \tag{7b}$$

$$\gamma_{x\theta} = \gamma^0_{x\theta} + z\kappa_{x\theta} = \left(\frac{1}{R}\frac{\partial u}{\partial \theta} + \frac{\partial v}{\partial x}\right) - z\left(\frac{2}{R}\frac{\partial^2 w}{\partial x \partial \theta}\right). \tag{7c}$$

One thing to emphasize here is that $\gamma_{x\theta} = 2\varepsilon_{x\theta}$. According to plane stress condition in thin shells ($\sigma_{zz} = 0$), by inserting Eqs. (7a)–(7c) into Eq. (2), one can get:

$$\varepsilon_{zz} = -\frac{\nu}{1-\nu}\left(\varepsilon^0_{xx} + \varepsilon^0_{\theta\theta}\right) - z\frac{\nu}{1-\nu}\left(\kappa_{xx} + \kappa_{\theta\theta}\right) + \frac{1+\nu}{1-\nu}\alpha\vartheta. \tag{8}$$

Substitution of Eqs. (7a)–(7c) and (8) into Eq. (2) results in the following nonlocal thermoelastic constitutive relations:

$$\left(1-\mu\nabla^2\right)\sigma_{xx} = \frac{E}{1-\nu^2}\left[\left(\varepsilon^0_{xx} + \nu\varepsilon^0_{\theta\theta}\right) + z\left(\kappa_{xx} + \nu\kappa_{\theta\theta}\right)\right] - \frac{E\alpha}{1-\nu}\vartheta, \tag{9a}$$

$$\left(1-\mu\nabla^2\right)\sigma_{\theta\theta} = \frac{E}{1-\nu^2}\left[\left(\nu\varepsilon^0_{xx} + \varepsilon^0_{\theta\theta}\right) + z\left(\nu\kappa_{xx} + \kappa_{\theta\theta}\right)\right] - \frac{E\alpha}{1-\nu}\vartheta, \tag{9b}$$

$$\left(1-\mu\nabla^2\right)\sigma_{x\theta} = \frac{E}{2(1+\nu)}\left[\left(\gamma^0_{x\theta} + z\kappa_{x\theta}\right)\right]. \tag{9c}$$

Note that $\nabla^2 = \left(\partial^2/\partial x^2\right) + \left(1/R^2\right)\left(\partial^2/\partial\theta^2\right)$.

Through the relations below, one can attain membrane force and bending moment resultants:

$$\left(N_{xx}, N_{\theta\theta}, N_{x\theta}\right) = \int_{-h/2}^{+h/2}\left(\sigma_{xx}, \sigma_{\theta\theta}, \sigma_{x\theta}\right)\mathrm{d}z, \tag{10a}$$

$$\left(M_{xx}, M_{\theta\theta}, M_{x\theta}\right) = \int_{-h/2}^{+h/2} z\left(\sigma_{xx}, \sigma_{\theta\theta}, \sigma_{x\theta}\right)\mathrm{d}z. \tag{10b}$$

By making use of Eqs. (9a)–(9c) and (10a)–(10b), the following relations of resultants are obtained:

$$\begin{aligned}\left(1-\mu\nabla^2\right)N_{xx} &= \frac{Eh}{1-\nu^2}\left(\varepsilon^0_{xx} + \nu\varepsilon^0_{\theta\theta}\right) - \frac{N_T}{1-\nu} \\ &= \frac{Eh}{1-\nu^2}\left(\frac{\partial u}{\partial x} + \frac{\nu}{R}\frac{\partial v}{\partial \theta} + \frac{\nu w}{R}\right) - \frac{N_T}{1-\nu},\end{aligned} \tag{11a}$$

$$\begin{aligned}\left(1-\mu\nabla^2\right)N_{\theta\theta} &= \frac{Eh}{1-\nu^2}\left(\nu\varepsilon^0_{xx} + \varepsilon^0_{\theta\theta}\right) - \frac{N_T}{1-\nu} \\ &= \frac{Eh}{1-\nu^2}\left(\nu\frac{\partial u}{\partial x} + \frac{1}{R}\frac{\partial v}{\partial \theta} + \frac{w}{R}\right) - \frac{N_T}{1-\nu},\end{aligned} \tag{11b}$$

$$\left(1-\mu\nabla^2\right)N_{x\theta} = \frac{Eh}{2(1+\nu)}\gamma^0_{x\theta} = \frac{Eh}{2(1+\nu)}\left(\frac{1}{R}\frac{\partial u}{\partial \theta} + \frac{\partial v}{\partial x}\right), \tag{11c}$$

and

$$\begin{aligned}\left(1-\mu\nabla^2\right)M_{xx} &= D\left(\kappa_{xx} + \nu\kappa_{\theta\theta}\right) - \frac{M_T}{1-\nu} \\ &= -D\left(\frac{\partial^2 w}{\partial x^2} + \frac{\nu}{R^2}\frac{\partial^2 w}{\partial \theta^2}\right) - \frac{M_T}{1-\nu},\end{aligned} \tag{12a}$$

$$\begin{aligned}\left(1-\mu\nabla^2\right)M_{\theta\theta} &= D\left(\nu\kappa_{xx} + \kappa_{\theta\theta}\right) - \frac{M_T}{1-\nu} \\ &= -D\left(\nu\frac{\partial^2 w}{\partial x^2} + \frac{1}{R^2}\frac{\partial^2 w}{\partial \theta^2}\right) - \frac{M_T}{1-\nu},\end{aligned} \tag{12b}$$

$$\left(1-\mu\nabla^2\right)M_{x\theta}=\frac{D(1-\nu)}{2}\kappa_{x\theta}=-D(1-\nu)\left(\frac{1}{R}\frac{\partial^2 w}{\partial x\partial\theta}\right), \tag{12c}$$

in which $D=Eh^3/12(1-\nu^2)$ is called bending rigidity of shell. Thermal force N_T and thermal moment M_T are also given by:

$$N_T=E\alpha\int_{-h/2}^{+h/2}\vartheta\mathrm{d}z \quad \text{and} \quad M_T=E\alpha\int_{-h/2}^{+h/2}\vartheta z\mathrm{d}z. \tag{13}$$

Transverse motion of a circular cylindrical shell is governed by the equation below [36]:

$$\frac{\partial^2 M_{xx}}{\partial x^2}+\frac{2}{R}\frac{\partial^2 M_{x\theta}}{\partial x\partial\theta}+\frac{1}{R^2}\frac{\partial^2 M_{\theta\theta}}{\partial\theta^2}-\frac{N_{\theta\theta}}{R}=\rho h\frac{\partial^2 w}{\partial t^2}. \tag{14}$$

By merging Eqs. (12a)–(12c) and (14), one can obtain:

$$D\nabla^4 w+\frac{1}{1-\nu}\nabla^2 M_T+\left(1-\mu\nabla^2\right)\frac{N_{\theta\theta}}{R}+\rho h\left(1-\mu\nabla^2\right)\frac{\partial^2 w}{\partial t^2}=0, \tag{15}$$

where symbol $\nabla^4=\nabla^2\left(\nabla^2\right)=(\partial^4/\partial x^4)+(2/R^2)(\partial^4/\partial x^2\partial\theta^2)+(1/R^4)(\partial^4/\partial\theta^4)$ represents the biharmonic operator. It is important to point up that the difference between equation above and that determined by Lu et al. [14] is due to different definitions of thermal resultants.

Owing to transverse deflection-dominated oscillations in DMV model of thin shells, one can neglect the influence of inertia in the in-plane direction. Accordingly, motion equations in longitudinal and circumferential directions can be written as [36]:

$$\frac{\partial N_{xx}}{\partial x}+\frac{1}{R}\frac{\partial N_{x\theta}}{\partial\theta}=0 \quad \text{and} \quad \frac{\partial N_{x\theta}}{\partial x}+\frac{1}{R}\frac{\partial N_{\theta\theta}}{\partial\theta}=0. \tag{16}$$

Airy function ϕ is defined as below:

$$N_{xx}=\frac{1}{R^2}\frac{\partial^2\phi}{\partial\theta^2}, \quad N_{x\theta}=-\frac{1}{R}\frac{\partial^2\phi}{\partial x\partial\theta}, \quad N_{\theta\theta}=\frac{\partial^2\phi}{\partial x^2}. \tag{17}$$

As it is evident, relations above satisfy motion Eqs. (16) completely. Substitution of Eq. (17) into Eq. (15) yields the transverse motion equation as follows:

$$D\nabla^4 w+\frac{1}{1-\nu}\nabla^2 M_T+\left(1-\mu\nabla^2\right)\nabla_K^2\phi+\rho h\left(1-\mu\nabla^2\right)\frac{\partial^2 w}{\partial t^2}=0, \tag{18}$$

with $\nabla_K^2=(1/R)\left(\partial^2/\partial x^2\right)$.

3.2 Compatibility equation

The compatibility equation of a circular cylindrical shell is given by [36]:

$$\frac{\partial}{\partial x}\left(R\frac{\partial\varepsilon_{\theta\theta}^0}{\partial x}-\frac{1}{2}\frac{\partial\gamma_{x\theta}^0}{\partial\theta}\right)+\frac{\partial}{\partial\theta}\left(\frac{1}{R}\frac{\partial\varepsilon_{xx}^0}{\partial\theta}-\frac{1}{2}\frac{\partial\gamma_{x\theta}^0}{\partial x}\right)+\kappa_{xx}=0. \tag{19}$$

With the aid of Eqs. (11a)–(11c), one can readily obtain:

$$\varepsilon_{xx}^0=\frac{1}{Eh}\left[\left(1-\mu\nabla^2\right)N_{xx}-\nu\left(1-\mu\nabla^2\right)N_{\theta\theta}+N_T\right], \tag{20a}$$

$$\varepsilon_{\theta\theta}^0=\frac{1}{Eh}\left[\left(1-\mu\nabla^2\right)N_{\theta\theta}-\nu\left(1-\mu\nabla^2\right)N_{xx}+N_T\right], \tag{20b}$$

$$\gamma_{x\theta}^0=\frac{2(1+\nu)}{Eh}[(1-\mu\nabla^2)N_{x\theta}], \tag{20c}$$

By inserting relations above into Eq. (19) and employing Eq. (17), the compatibility equation takes the following form:

$$\left(1-\mu\nabla^2\right)\nabla^4\phi+\nabla^2 N_T-Eh\nabla_K^2 w=0. \tag{21}$$

3.3 Heat conduction equation

By means of Eqs. (7a), (7b) and (8), one can determine cubical dilatation ε_{mm} as:

$$\varepsilon_{mm}=\frac{1-2\nu}{1-\nu}\left[\left(\varepsilon_{xx}^0+\varepsilon_{\theta\theta}^0\right)+z\left(\kappa_{xx}+\kappa_{\theta\theta}\right)\right]+\frac{1+\nu}{1-\nu}\alpha\vartheta. \tag{22}$$

Substitution of Eqs. (7a), (7b), (20a) and (20b) into relation above leads to:

$$\varepsilon_{mm}=\frac{1}{Eh}\frac{1-2\nu}{1-\nu}\left[(1-\nu)\left(1-\mu\nabla^2\right)\left(N_{xx}+N_{\theta\theta}\right)+2N_T\right]-\frac{1-2\nu}{1-\nu}z\nabla^2 w+\frac{1+\nu}{1-\nu}\alpha\vartheta. \tag{23}$$

Given scant impact of thermoelastic coupling, the magnitude of N_T is much lower than that of $N_{xx}+N_{\theta\theta}$ [14]. By taking into consideration this point and utilizing Eq. (17) into (23), cubical dilatation becomes:

$$\varepsilon_{mm}=\frac{1-2\nu}{Eh}\left(1-\mu\nabla^2\right)\nabla^2\phi-\frac{1-2\nu}{1-\nu}z\nabla^2 w+\frac{1+\nu}{1-\nu}\alpha\vartheta. \tag{24}$$

For circular cylindrical shells, three-dimensional Laplace operator $\overline{\nabla}^2$ is expressed by:

$$\overline{\nabla}^2=\frac{\partial^2}{\partial x^2}+\frac{1}{(R+z)^2}\frac{\partial^2}{\partial\theta^2}+\frac{\partial^2}{\partial z^2}+\frac{1}{R+z}\frac{\partial}{\partial z}. \tag{25}$$

In thin circular cylindrical shells, thickness value is trivial compared to radius value (i.e. $R\gg z$). Additionally, in thin mechanical elements, temperature gradients in transverse direction are enormous in comparison with those in other

directions [14]. On account of these two significant issues, one can write:

$$\overline{\nabla}^2\vartheta = \frac{\partial^2\vartheta}{\partial z^2} + \frac{1}{R}\frac{\partial\vartheta}{\partial z}. \tag{26}$$

Substitution of Eqs. (24) and (26) into Eq. (5) and simplification of result gives:

$$\begin{aligned}\chi\left(1+\tau_T\frac{\partial}{\partial t}\right)\left(\frac{\partial^2\vartheta}{\partial z^2}+\frac{1}{R}\frac{\partial\vartheta}{\partial z}\right)&=\left[1+\Delta_E\frac{1+\nu}{(1-2\nu)(1-\nu)}\right]\left(1+\tau_q\frac{\partial}{\partial t}\right)\frac{\partial\vartheta}{\partial t}\\&+\frac{\Delta_E}{\alpha Eh}\left(1+\tau_q\frac{\partial}{\partial t}\right)\frac{\partial}{\partial t}\left(1-\mu\nabla^2\right)\nabla^2\phi\\&-\frac{\Delta_E}{\alpha(1-\nu)}\left(1+\tau_q\frac{\partial}{\partial t}\right)\frac{\partial}{\partial t}\left(z\nabla^2 w\right),\end{aligned} \tag{27}$$

with $\chi = k/\rho c_v$ and $\Delta_E = E\alpha^2 T_0/\rho c_v$ standing for thermal diffusivity and relaxation strength, respectively. Since the value of relaxation strength is typically trifling ($\Delta_E \ll 1$), one can simplify heat conduction Eq. (27) as follows:

$$\begin{aligned}\chi\left(1+\tau_T\frac{\partial}{\partial t}\right)\left(\frac{\partial^2\vartheta}{\partial z^2}+\frac{1}{R}\frac{\partial\vartheta}{\partial z}\right)&=\left(1+\tau_q\frac{\partial}{\partial t}\right)\frac{\partial\vartheta}{\partial t}+\frac{\Delta_E}{\alpha Eh}\left(1+\tau_q\frac{\partial}{\partial t}\right)\frac{\partial}{\partial t}\left(1-\mu\nabla^2\right)\nabla^2\phi\\&-\frac{\Delta_E}{\alpha(1-\nu)}\left(1+\tau_q\frac{\partial}{\partial t}\right)\frac{\partial}{\partial t}\left(z\nabla^2 w\right).\end{aligned} \tag{28}$$

4 Determination of TED value

Asymmetric time-harmonic vibrations are adopted for circular cylindrical shell as below:

$$w(x,\theta,t) = \sum_{m=1}^{\infty}\sum_{n=0}^{\infty} W_m(x)\mathrm{e}^{i(\omega_{mn}t+n\theta)}, \tag{29a}$$

$$\vartheta(x,\theta,z,t) = \sum_{m=1}^{\infty}\sum_{n=0}^{\infty} \Theta_m(x,z)\mathrm{e}^{i(\omega_{mn}t+n\theta)}, \tag{29b}$$

$$\phi(x,\theta,t) = \sum_{m=1}^{\infty}\sum_{n=0}^{\infty} \Phi_m(x)\mathrm{e}^{i(\omega_{mn}t+n\theta)}, \tag{29c}$$

where ω_{mn} shows the complex frequency comprising thermoelastic coupling effect. By inserting relations above into Eq. (28), one can arrive at the following heat conduction equation:

$$\begin{aligned}&\frac{\partial^2\Theta_m}{\partial z^2}+\frac{1}{R}\frac{\partial\Theta_m}{\partial z}+p^2\Theta_m\\&=p^2\frac{\Delta_E}{\alpha(1-\nu)}z\nabla_1^2 W_m-p^2\frac{\Delta_E}{\alpha Eh}\left(1-\mu\nabla_1^2\right)\nabla_1^2\Phi_m,\end{aligned} \tag{30}$$

in which $\nabla_1^2 = \left(\mathrm{d}^2/\mathrm{d}x^2\right) - (n^2/R^2)$. Moreover, complex parameter p is introduced by:

$$\begin{aligned}&p = \sqrt{\frac{\omega_{mn}}{\chi}}\sqrt{a_1 - ia_2} \quad \text{with}\\&a_1 = \frac{\left(\tau_q-\tau_T\right)\omega_{mn}}{1+\tau_T^2\omega_{mn}^2} \quad \text{and} \quad a_2 = \frac{1+\tau_T\tau_q\omega_{mn}^2}{1+\tau_T^2\omega_{mn}^2}.\end{aligned} \tag{31}$$

General solution of Eq. (30) is expressed by:

$$\begin{aligned}\Theta_m(x,z) = c_1\mathrm{e}^{r_1 z} + c_2\mathrm{e}^{r_2 z} + \frac{\Delta_E}{\alpha(1-\nu)}\left(z-\frac{1}{R}\frac{1}{p^2}\right)\nabla_1^2 W_m\\-\frac{\Delta_E}{\alpha Eh}\left(1-\mu\nabla_1^2\right)\nabla_1^2\Phi_m,\end{aligned} \tag{32}$$

where c_1 and c_2 are unknown coefficients to be specified via thermal boundary conditions. Additionally, parameters r_1 and r_2 are determined by:

$$r_1 = \frac{-1+\sqrt{1-4R^2p^2}}{2R} \quad \text{and} \quad r_2 = \frac{-1-\sqrt{1-4R^2p^2}}{2R}. \tag{33}$$

By taking adiabatic boundary conditions at the internal and external surfaces of nanoshell, one can write $\partial\Theta_m/\partial z = 0$ at $z = \pm h/2$. According to these thermal boundary conditions, the solution of temperature change appeared in Eq. (32) becomes:

$$\begin{aligned}\Theta_m(x,z) = \frac{\Delta_E}{\alpha(1-\nu)}\left[\frac{1}{r_1}\frac{\sinh\left(r_2h/2\right)}{\sinh[\left(r_1-r_2\right)h/2]}\mathrm{e}^{r_1 z} - \frac{1}{r_2}\frac{\sinh\left(r_1h/2\right)}{\sinh[\left(r_1-r_2\right)h/2]}\mathrm{e}^{r_2 z}\right.\\\left.+z-\frac{1}{R}\frac{1}{p^2}\right]\nabla_1^2 W_m - \frac{\Delta_E}{\alpha Eh}\left(1-\mu\nabla_1^2\right)\nabla_1^2\Phi_m.\end{aligned} \tag{34}$$

Substitution of relation above into relations of Eq. (13) gives:

$$N_T = \sum_{m=1}^{\infty}\sum_{n=0}^{\infty} N_{T,m}(x)\mathrm{e}^{i(\omega_{mn}t+n\theta)}, \tag{35a}$$

$$M_T = \sum_{m=1}^{\infty}\sum_{n=0}^{\infty} M_{T,m}(x)\mathrm{e}^{i(\omega_{mn}t+n\theta)}, \tag{35b}$$

in which

$$\begin{aligned}N_{T,m} = \frac{E\Delta_E}{1-\nu}\left[\frac{2\sinh\left(r_1h/2\right)\sinh\left(r_2h/2\right)}{\sinh[\left(r_1-r_2\right)h/2]}\left(\frac{1}{r_1^2}-\frac{1}{r_2^2}\right)-\frac{h}{R}\frac{1}{p^2}\right]\nabla_1^2 W_m\\-\Delta_E\left(1-\mu\nabla_1^2\right)\nabla_1^2\Phi_m,\end{aligned} \tag{36a}$$

$$M_{T,m} = \frac{E\Delta_E}{1-\nu}\left[\frac{h^3}{12} + \frac{1}{r_1}\frac{\sinh\left(r_2 h/2\right)}{\sinh[\left(r_1 - r_2\right)h/2]}f\left(r_1\right) - \frac{1}{r_2}\frac{\sinh\left(r_1 h/2\right)}{\sinh[\left(r_1 - r_2\right)h/2]}f\left(r_2\right)\right]\nabla_1^2 W_m, \tag{36b}$$

with

$$f(r) = \frac{h}{r}\cosh\left(rh/2\right) - \frac{2}{r^2}\sinh\left(rh/2\right). \tag{37}$$

Substitution of Eq. (36b) into motion Eq. (18) gives:

$$\left[D + \Delta_E F\left(\omega_{mn}\right)\right]\nabla_1^4 W_m + \left(1 - \mu\nabla_1^2\right)\nabla_K^2\Phi_m - \rho h\omega_{mn}^2\left(1 - \mu\nabla_1^2\right)W_m = 0, \tag{38}$$

with $\nabla_1^4 = \nabla_1^2\left(\nabla_1^2\right) = \left(\mathrm{d}^4/\mathrm{d}x^4\right) - 2\left(n^2/R^2\right)\left(\mathrm{d}^2/\mathrm{d}x^2\right) + \left(n^4/R^4\right)$. Furthermore:

$$F\left(\omega_{mn}\right) = \frac{Eh^3}{12(1-\nu)^2}\left\{1 + \frac{12}{h^3}\left[\frac{1}{r_1}\frac{\sinh\left(r_2 h/2\right)}{\sinh[\left(r_1 - r_2\right)h/2]}f\left(r_1\right) - \frac{1}{r_2}\frac{\sinh\left(r_1 h/2\right)}{\sinh[\left(r_1 - r_2\right)h/2]}f\left(r_2\right)\right]\right\}. \tag{39}$$

By inserting Eq. (36a) into compatibility Eq. (21), one can get:

$$\Delta_E G\left(\omega_{mn}\right)\nabla_1^4 W_m + \left(1 - \mu\nabla_1^2\right)\nabla_1^4\Phi_m - Eh\nabla_K^2 W_m = 0, \tag{40}$$

where

$$G\left(\omega_{mn}\right) = \frac{E}{1-\nu}\left[\frac{2\sinh\left(r_1 h/2\right)\sinh\left(r_2 h/2\right)}{\sinh[\left(r_1 - r_2\right)h/2]}\left(\frac{1}{r_1^2} - \frac{1}{r_2^2}\right) - \frac{h}{R}\frac{1}{p^2}\right]. \tag{41}$$

Elimination of function Φ_m from Eqs. (38) and (40) provides the thermoelastic frequency equation in terms of W_m as below:

$$\left[D + \Delta_E F\left(\omega_{mn}\right)\right]\nabla_1^8 W_m - \Delta_E G\left(\omega_{mn}\right)\nabla_K^2\nabla_1^4 W_m + Eh\nabla_K^4 W_m = \rho h\omega_{mn}^2\left(1 - \mu\nabla_1^2\right)\nabla_1^4 W_m, \tag{42}$$

in which $\nabla_K^4 = \nabla_K^2\left(\nabla_K^2\right) = \left(1/R^2\right)\left(\mathrm{d}^4/\mathrm{d}x^4\right)$. In addition:

$$\nabla_1^8 = \nabla_1^4\left(\nabla_1^4\right) = \frac{\mathrm{d}^8}{\mathrm{d}x^8} - 4\frac{n^2}{R^2}\frac{\mathrm{d}^6}{\mathrm{d}x^6} + 6\frac{n^4}{R^4}\frac{\mathrm{d}^4}{\mathrm{d}x^4} - 4\frac{n^6}{R^6}\frac{\mathrm{d}^2}{\mathrm{d}x^2} + \frac{n^8}{R^8}. \tag{43}$$

In the absence of thermoelastic coupling effect, Eq. (42) reduces to isothermal frequency equation as follows:

$$D\nabla_1^8 W_m + Eh\nabla_K^4 W_m = \rho h\omega_{0,mn}^2\left(1 - \mu\nabla_1^2\right)\nabla_1^4 W_m, \tag{44}$$

where $\omega_{0,mn}$ refers to the nonlocal isothermal frequency of mode number (m, n). For arbitrary boundary conditions, the Galerkin method is applied on equation above to determine the approximate value of $\omega_{0,mn}$ as [36]:

$$\omega_{0,mn} = \left[\frac{D\int_0^L W_m\nabla_1^8 W_m\mathrm{d}x + Eh\int_0^L W_m\nabla_K^4 W_m\mathrm{d}x}{\rho h\int_0^L W_m\left(1 - \mu\nabla_1^2\right)\nabla_1^4 W_m\mathrm{d}x}\right]^{\frac{1}{2}}. \tag{45}$$

Beam mode shapes are a common selection of shape function W_m for rectangular plates and cylindrical shells [36]. For a nonlocal beam, the governing equation of mode shape is given by:

$$\frac{\mathrm{d}^4 W_m}{\mathrm{d}x^4} = \lambda_m^4\left(1 - \mu\frac{\mathrm{d}^2}{\mathrm{d}x^2}\right)W_m, \tag{46}$$

in which λ_m are the roots of beam eigenvalue problem. It is important to emphasize that the boundary conditions of the beam should be same as those of the shell. Additional explanations about the mode shape of different boundary conditions are provided in Appendix section. Given that thermoelastic coupling effect is marginal, one can replace $F\left(\omega_{mn}\right)$ and $G\left(\omega_{mn}\right)$ with $F(\omega_{0,mn})$ and $G(\omega_{0,mn})$ in Eq. (42) [14]. Accordingly, the frequency equation takes the following form:

$$\left[D + \Delta_E F\left(\omega_{0,mn}\right)\right]\nabla_1^8 W_m - \Delta_E G\left(\omega_{0,mn}\right)\nabla_K^2\nabla_1^4 W_m + Eh\nabla_K^4 W_m = \rho h\omega_{mn}^2\left(1 - \mu\nabla_1^2\right)\nabla_1^4 W_m. \tag{47}$$

Implementation of the Galerkin procedure in Eq. (47) and segregation of real and imaginary parts gives:

$$\omega_{mn}^2 = \varphi_{mn} + i\psi_{mn}, \tag{48}$$

where

$$\varphi_{mn} = \frac{\left(D + \Delta_E F_r\right)\int_0^L W_m\nabla_1^8 W_m\mathrm{d}x - \Delta_E G_r\int_0^L W_m\nabla_K^2\nabla_1^4 W_m\mathrm{d}x + Eh\int_0^L W_m\nabla_K^4 W_m\mathrm{d}x}{\rho h\int_0^L W_m\left(1 - \mu\nabla_1^2\right)\nabla_1^4 W_m\mathrm{d}x}, \tag{49a}$$

$$\psi_{mn}=\frac{\Delta_E F_i\int_0^L W_m\nabla_1^8 W_m\mathrm{d}x-\Delta_E G_i\int_0^L W_m\nabla_K^2\nabla_1^4 W_m\mathrm{d}x}{\rho h\int_0^L W_m\left(1-\mu\nabla_1^2\right)\nabla_1^4 W_m\mathrm{d}x}, \tag{49b}$$

in which functions F_r and F_i denote the real and imaginary parts of $F\left(\omega_{0,mn}\right)$, respectively. Additionally, functions G_r and G_i represent the real and imaginary parts of $G\left(\omega_{0,mn}\right)$, respectively. According to the complex frequency approach, TED value is determined via the following relation [13]:

$$Q^{-1}=2\left|\frac{Im\left(\omega_{mn}\right)}{Re\left(\omega_{mn}\right)}\right|. \tag{50}$$

By referring to Eq. (48) and conducting a procedure similar to what has been performed in [37], one can write:

$$Q^{-1}=\left|\frac{\psi_{mn}}{\varphi_{mn}}\right|. \tag{51}$$

By inserting Eqs. (49a) and (49b) into equation above, the expression estimating TED becomes:

$$Q^{-1}=\left|\frac{\Delta_E F_i\int_0^L W_m\nabla_1^8 W_m\mathrm{d}x-\Delta_E G_i\int_0^L W_m\nabla_K^2\nabla_1^4 W_m\mathrm{d}x}{\left(D+\Delta_E F_r\right)\int_0^L W_m\nabla_1^8 W_m\mathrm{d}x-\Delta_E G_r\int_0^L W_m\nabla_K^2\nabla_1^4 W_m\mathrm{d}x+Eh\int_0^L W_m\nabla_K^4 W_m\mathrm{d}x}\right|. \tag{52}$$

Owing to small value of relaxation strength Δ_E, Eq. (52) can be simplified to the following relation:

$$Q^{-1}=\left|\frac{\Delta_E F_i\int_0^L W_m\nabla_1^8 W_m\mathrm{d}x-\Delta_E G_i\int_0^L W_m\nabla_K^2\nabla_1^4 W_m\mathrm{d}x}{D\int_0^L W_m\nabla_1^8 W_m\mathrm{d}x+Eh\int_0^L W_m\nabla_K^4 W_m\mathrm{d}x}\right|. \tag{53}$$

With the help of relation above, one can predict the magnitude of TED in circular cylindrical shells by capturing nonlocal and dual-phase-lagging effect.

5 Explicit solution to TED in simply supported cylindrical shells

In this section, an explicit solution for TED in a simply supported cylindrical nanoshell is presented. For such a shell, the boundary conditions at the edges $x=0$ and $x=L$ are expressed as [36]:

$$w=v=M_{xx}=N_{xx}=0. \tag{54}$$

Accordingly, the Navier solution is considered to represent displacement field as below:

$$u(x,\theta,t)=\sum_{m=1}^{\infty}\sum_{n=0}^{\infty}A_m\cos\left(\frac{m\pi x}{L}\right)\cos n(\theta-\gamma)\mathrm{e}^{i\omega_{mn}t}, \tag{55a}$$

$$v(x,\theta,t)=\sum_{m=1}^{\infty}\sum_{n=0}^{\infty}B_m\sin\left(\frac{m\pi x}{L}\right)\sin n(\theta-\gamma)\mathrm{e}^{i\omega_{mn}t}, \tag{55b}$$

$$w(x,\theta,t)=\sum_{m=1}^{\infty}\sum_{n=0}^{\infty}C_m\sin\left(\frac{m\pi x}{L}\right)\cos n(\theta-\gamma)\mathrm{e}^{i\omega_{mn}t}. \tag{55c}$$

Hence, one can write:

$$W_m(x)=C_m\sin\left(\frac{m\pi x}{L}\right). \tag{56}$$

The Navier solution presented in Eqs. (55a)–(55c) is fully compatible with boundary conditions given in Eq. (54). Moreover, the shape function presented in Eq. (56) satisfies both isothermal frequency Eq. (44) and coupled thermoelastic frequency Eq. (47). In consequence, Eqs. (55a)–(55c) are the exact solutions of TED problem for simply supported cylindrical shells. Substitution of Eq. (56) into isothermal frequency Eq. (44) gives:

Table 1 Mechanical and thermal constants of single-walled carbon nanotube (SWCN) at $T_0=300\mathrm{K}$ [14]

E(GPa)	ν	$\rho(\mathrm{kgm}^{-3})$	$k(\mathrm{Wm}^{-1}\mathrm{K}^{-1})$	$\alpha(10^{-6}\mathrm{K}^{-1})$	$\rho c_v(10^6\mathrm{Jm}^{-3}\mathrm{K}^{-1})$
1060	0.25	2270	2000	7	1.36

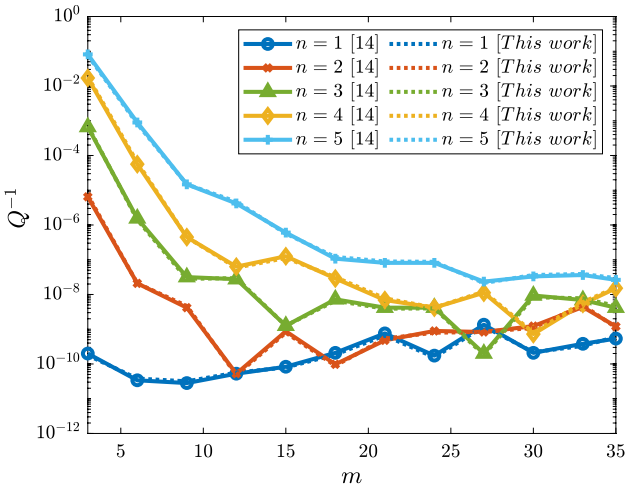

Fig. 2 Effect of vibration modes on TED in a clamped–clamped single-walled carbon nanotube (SWCN) with geometrical properties $R = 70$nm, $L = 350$nm and $h = 0.35$nm

Table 2 Thermoelastic properties of some materials at $T_0 = 300$K [10]

Material property	Copper (Cu)	Gold (Au)	Lead (Pb)
E(GPa)	110	79	16
ν	0.35	0.40	0.44
ρ(kgm^{-3})	8940	19,300	11,340
k(Wm^{-1}K^{-1})	386	315	35.3
α(10^{-6}K^{-1})	16.5	14.2	28.9
c_v(Jkg^{-1}K^{-1})	385.9	129.1	128
τ_q(ps)	0.4348	0.7438	0.1670
τ_T(ps)	70.833	89.286	12.097

$$\omega_{0,mn} = \left[\frac{D\left[\left(\frac{m\pi}{L}\right)^2 + \left(\frac{n}{R}\right)^2\right]^4 + \frac{Eh}{R^2}\left(\frac{m\pi}{L}\right)^4}{\rho h\left[\left(\frac{m\pi}{L}\right)^2 + \left(\frac{n}{R}\right)^2\right]^2 \left\{1 + \mu\left[\left(\frac{m\pi}{L}\right)^2 + \left(\frac{n}{R}\right)^2\right]\right\}} \right]^{\frac{1}{2}}. \tag{57}$$

In addition, by inserting Eq. (56) into coupled thermoelastic frequency Eq. (47) and doing the same procedure conducted in the previous section, the explicit relation of TED in simply supported circular cylindrical nanoshells can be readily derived as follows:

$$Q^{-1} = \left| \frac{\Delta_E F_i\left[\left(\frac{m\pi}{L}\right)^2 + \left(\frac{n}{R}\right)^2\right]^4 + \Delta_E \frac{G_i}{R}\left[\left(\frac{m\pi}{L}\right)^2 + \left(\frac{n}{R}\right)^2\right]^2 \left(\frac{m\pi}{L}\right)^2}{D\left[\left(\frac{m\pi}{L}\right)^2 + \left(\frac{n}{R}\right)^2\right]^4 + \frac{Eh}{R^2}\left(\frac{m\pi}{L}\right)^4} \right|. \tag{58}$$

6 Numerical results and discussion

In this section, several graphical data and numerical results are given to examine size-dependent TED in cylindrical nanoshells. First, with the aim of assessment of the validity of presented model, a comparison study is performed between the results of current study and those reported in the literature. Next, by providing several numerical results, a detailed parametric study is made for the sake of clarifying the influence of some determining factors like nonlocal parameter, phase lags, vibration modes and material on TED value.

6.1 Comparison study

For the sake of checking the validity of given formulation, a comparison study is performed between the findings of this study with those of the research of Lu et al. [14]. They evaluated TED in thin circular cylindrical shells in the framework of classical continuum theory and Fourier heat conduction law. In consequence, nonclassical mechanical and thermal constants, i.e. μ, τ_q and τ_T should be ignored in the presented model to compare the outcomes of these two investigations. Thermoelastic properties of single-walled carbon nanotube (SWCN) are given in Table 1 [14]. For different mode numbers, the variation of TED predicted in [14] and estimated in current work is depicted in Fig. 2 for a clamped–clamped SWCN with geometrical parameters $R = 70$nm, $L = 350$nm and $h = 0.35$nm. As it is evident, the results extracted on the basis of developed formulation in this article are in good agreement with those reported by Lu et al. [14].

6.2 Parametric study

This section is devoted to appraisal of the impact of some key factors such as nonlocal parameter, phase lags and material on the magnitude of TED for some mode numbers. Except where specified, numerical examples are presented for a circular cylindrical shell made of copper with geometrical ratios $L/R = 4$ and $R/h = 60$. Thermoelastic constants of copper (Cu) as well as gold (Au) and lead (Pb) at reference temperature $T_0 = 300$K are listed in Table 2.

6.2.1 Impact of nonlocal parameter on TED

Figure 3 indicates the variation of normalized value of TED ((Q^{-1}/Δ_E)*(10^6)) as a function of the radius of nanoshell for different values of nonlocal parameter μ. It can be observed that for nano-sized cylindrical shells, as the magnitude of radius ascends, TED value gets larger. It is also inferred that nonlocal theory predicts greater values of TED in comparison with classical theory. As it is obvious, by increasing the nonlocal parameter μ, the amount of TED intensifies.

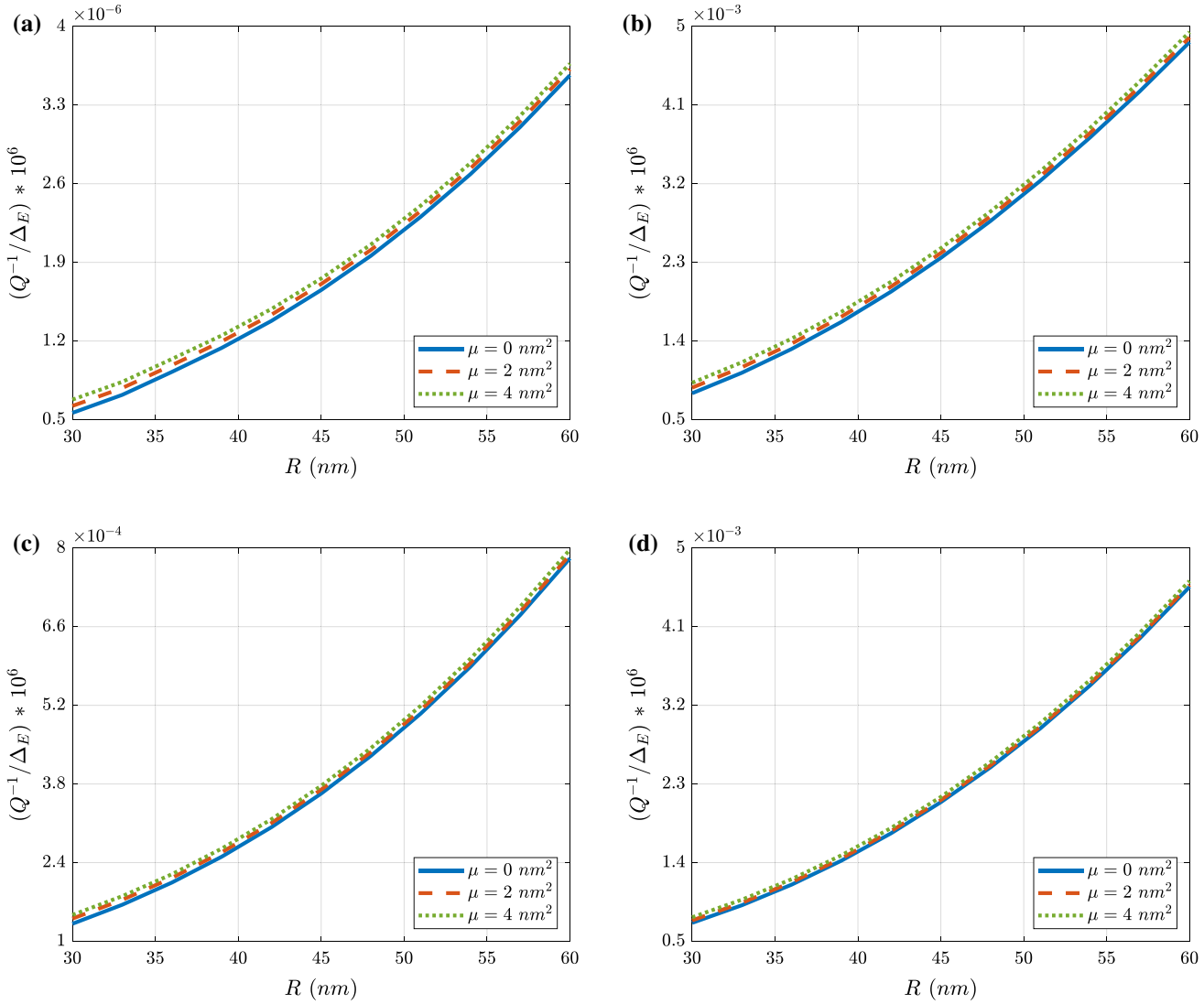

Fig. 3 Sensitivity of TED value to nonlocal parameter μ for some mode numbers **a** $(m, n) = (1, 0)$, **b** $(m, n) = (1, 1)$, **c** $(m, n) = (2, 0)$, **d** $(m, n) = (2, 1)$

To highlight the influence of nonlocal parameter on TED value, Fig. 4 depicts the nonlocal TED ratio ($Q^{-1}_{\text{Nonlocal}}/Q^{-1}_{\text{Local}}$) versus the radius of nanoshell. Based on these plots, one can deduce that by reduction of nanoshell's size, the nonlocal effect is reinforced. This outcome betokens the importance of size-dependency phenomenon at nanosacles. It is also apparent that when the radius of nanoshell increases, the nonlocal effect shrinks, so that the magnitude of TED predicted by nonlocal theory tends to that calculated by classical theory. Similar to what was seen in Fig. 3, for bigger amounts of nonlocal parameter μ, the nonlocal effect on TED value enlarges. In addition, as for the mode numbers examined in paper at hand, the maximum and minimum nonlocal effect belong to vibration modes $(m, n) = (1, 0)$ and $(m, n) = (2, 1)$, respectively.

6.2.2 Impact of DPL model on TED

Figure 5 compares normalized values of TED determined by means of CTE and DPL models versus the radius of nanoshell for some vibration modes. To plot these curves, the nonlocal parameter μ is assumed to be zero. As it is observed, in comparison with CTE model, utilization of DPL model leads to smaller amounts of TED. In addition, according to these curves, the highest and lowest thermoelastic damping take place in vibration modes $(m, n) = (2, 1)$ and $(m, n) = (1, 0)$, respectively.

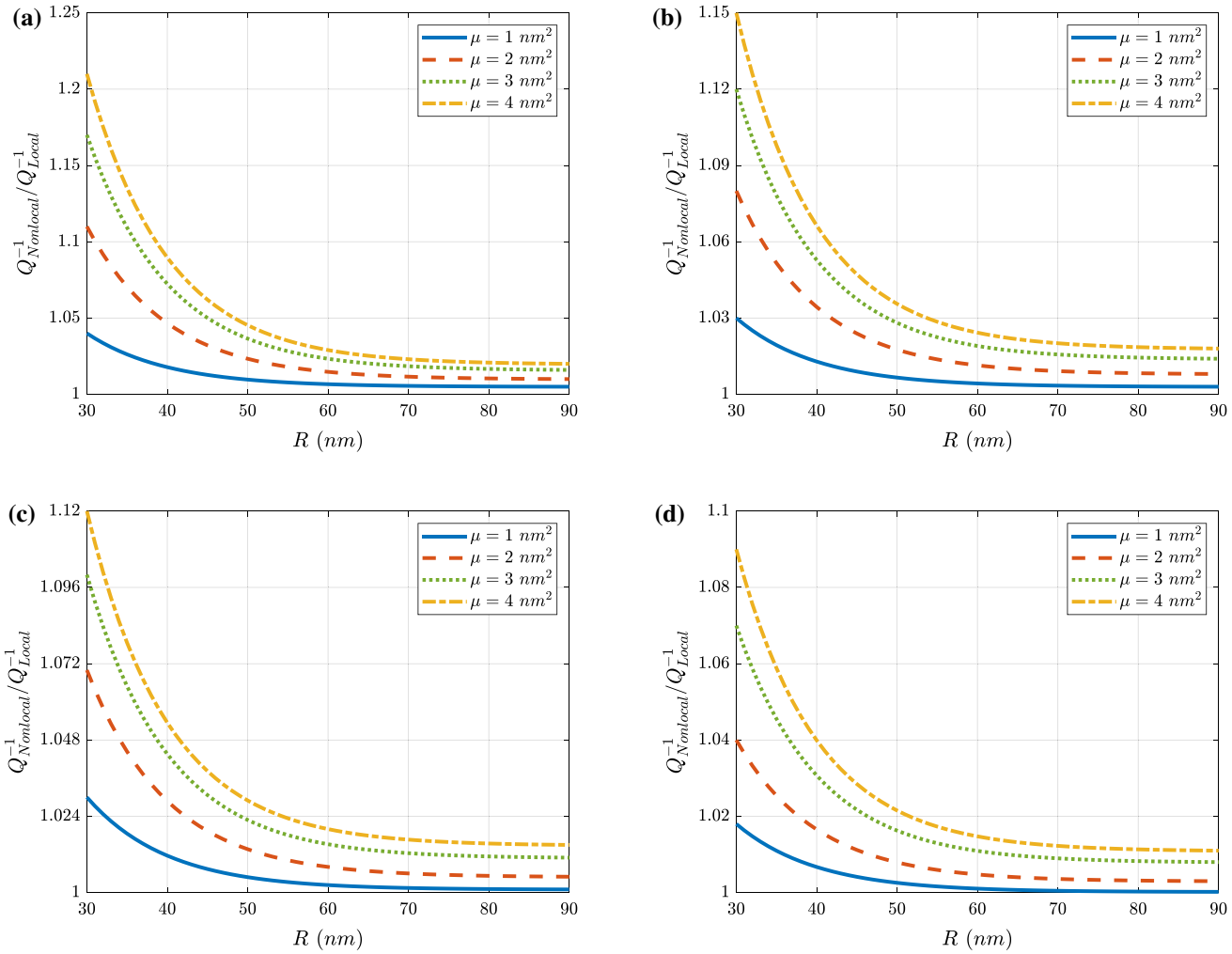

Fig. 4 Nonlocal TED ratio as a function of radius of cylindrical nanoshell for some mode numbers **a** $(m, n) = (1, 0)$, **b** $(m, n) = (1, 1)$, **c** $(m, n) = (2, 0)$, **d** $(m, n) = (2, 1)$

In Fig. 6, for four different mode numbers, the DPL TED ratio ($Q^{-1}_{\mathrm{DPL}}/Q^{-1}_{\mathrm{CTE}}$) as a function of nanoshell's radius is displayed to focus on the dual-phase-lagging effect on TED. The nonlocal parameter μ is again considered to be zero. It is apparent that by diminution in the radius of nanoshell, the effect of DPL model strengthens. This result reveals that DPL model has the means to capture small-scale effect in heat conduction process. It can be also easily seen that by increasing the dimensions of nanoshell, the predictions of DPL model converge to those of CTE model. Regarding the vibration modes, it is worth noting that the highest and lowest dual-phase-lagging effect occurs at mode numbers $(m, n) = (2, 0)$ and $(m, n) = (1, 1)$, respectively.

For some vibration modes, Fig. 7 illustrates the DPL TED ratio for a cylindrical nanoshell with fixed thickness $h = 5$nm and variable radius R and length L. The surfaces are plotted by taking $\mu = 0\mathrm{nm}^2$. It is clearly seen that by enlargement of radius or length of nanoshell, the impact of phase lags on TED dwindles, and the amount of TED anticipated by DPL model approaches that specified by CTE model. It is also observed that for axisymmetric vibration modes $(m, n) = (1, 0)$ and $(m, n) = (2, 0)$, the variation in the length of nanoshell doesn't lead to a meaningful change in the DPL TED ratio.

6.2.3 Impact of material on TED

The effect of material on TED in cylindrical nanoshells of radius $R = 45$nm is evaluated in Tables 3, 4 and 5 for some nonlocal parameters and mode numbers. On the basis of these numerical data, nanoshells made of lead and gold exhibit the most and least values of TED, respectively. It is also clear that in addition to nanoshells made of copper, the nonlocal effect augments TED value in nanoshells made of gold and lead.

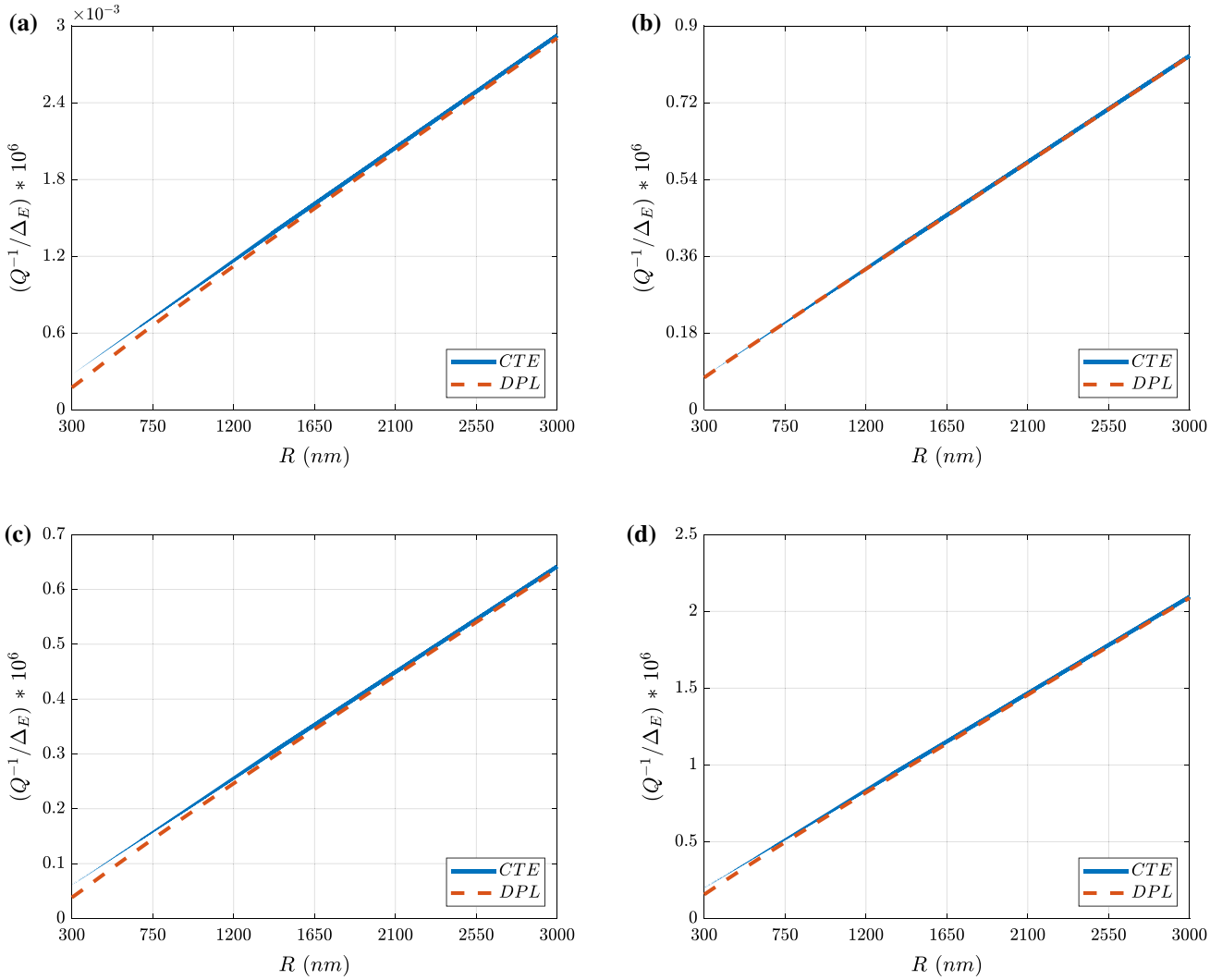

Fig. 5 Sensitivity of TED value to phase lags for some mode numbers **a** $(m,n) = (1,0)$, **b** $(m,n) = (1,1)$, **c** $(m,n) = (2,0)$, **d** $(m,n) = (2,1)$

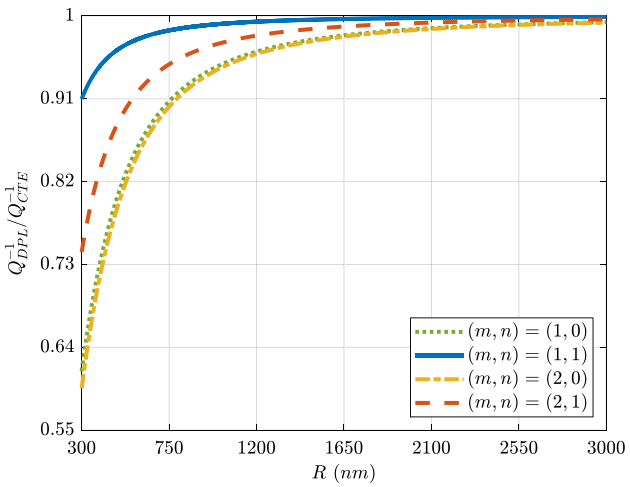

Fig. 6 DPL TED ratio as a function of radius of cylindrical nanoshell for some vibration modes

Table 6 reveals the dual-phase-lagging effect on TED in nanoshells made of copper, gold and lead for four different vibration modes. To extract these results, the radius of nanoshell is chosen as $R = 300$nm. The nonlocal parameter μ is also set to zero. According to DPL TED ratios, the maximum and minimum impact of dual-phase-lagging on TED belong to nanoshells made of copper and lead, respectively. Moreover, similar to copper, the greatest and smallest dual-phase-lagging effect on TED in nanoshells made of gold and lead is observed at vibration modes $(m,n) = (2,0)$ and $(m,n) = (1,1)$, respectively.

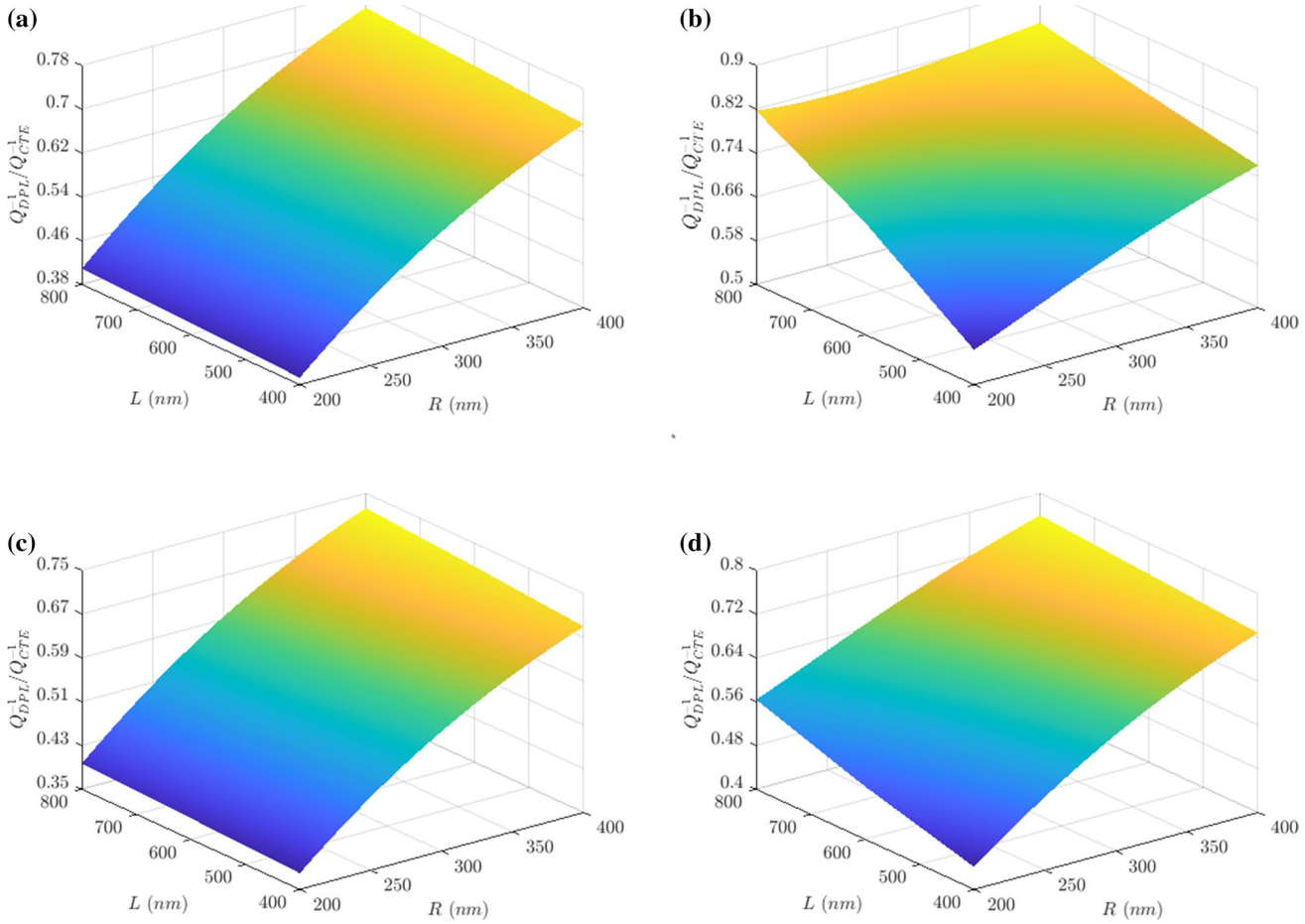

Fig. 7 Effect of length and radius on DPL TED ratio of a cylindrical shell with thickness $h = 5$nm for some vibration modes **a** $(m, n) = (1, 0)$, **b** $(m, n) = (1, 1)$, **c** $(m, n) = (2, 0)$, **d** $(m, n) = (2, 1)$

Table 3 Comparison of values of TED in cylindrical nanoshells made of copper for some mode numbers and nonlocal parameters

Mode number (m, n)	$\mu(\text{nm}^2)$	$Q^{-1} * (10^{15})$	$Q^{-1}_{\text{Nonlocal}}/Q^{-1}_{\text{Local}}$
(1, 0)	0	4.307	1
	2	4.462	1.036
	4	4.604	1.069
(1, 1)	0	6124	1
	2	6283	1.026
	4	6442	1.052
(2, 0)	0	945.2	1
	2	966.0	1.022
	4	984.9	1.042
(2, 1)	0	5448	1
	2	5519	1.013
	4	5622	1.032

Table 4 Comparison of values of TED in cylindrical nanoshells made of gold for some mode numbers and nonlocal parameters

Mode number (m, n)	$\mu(\text{nm}^2)$	$Q^{-1} * (10^{15})$	$Q^{-1}_{\text{Nonlocal}}/Q^{-1}_{\text{Local}}$
(1, 0)	0	1.690	1
	2	1.727	1.022
	4	1.763	1.043
(1, 1)	0	4419	1
	2	4494	1.017
	4	4574	1.035
(2, 0)	0	753.1	1
	2	762.1	1.012
	4	771.2	1.024
(2, 1)	0	4256	1
	2	4299	1.010
	4	4333	1.018

Table 5 Comparison of values of TED in cylindrical nanoshells made of lead for some mode numbers and nonlocal parameters

Mode number (m, n)	$\mu(\mathrm{nm}^2)$	$Q^{-1} * (10^{15})$	$Q^{-1}_{\mathrm{Nonlocal}}/Q^{-1}_{\mathrm{Local}}$
(1, 0)	0	396.707	1
	2	426.460	1.075
	4	458.197	1.155
(1, 1)	0	72,930.4	1
	2	77,160.4	1.058
	4	81,390.3	1.116
(2, 0)	0	53,230.1	1
	2	55,731.9	1.047
	4	58,393.4	1.097
(2, 1)	0	177,002	1
	2	183,551	1.037
	4	189,215	1.069

Table 6 Dual-phase-lagging effect on TED in cylindrical nanoshells for some materials and mode numbers

Material	Mode number (m, n)	$Q^{-1}_{\mathrm{DPL}} * (10^{13})$	$Q^{-1}_{\mathrm{CTE}} * (10^{13})$	$Q^{-1}_{\mathrm{DPL}}/Q^{-1}_{\mathrm{CTE}}$
Copper	(1, 0)	4.6809	7.6224	0.6141
	(1, 1)	1967.2	2162.2	0.9098
	(2, 0)	995.23	1671.0	0.5956
	(2, 1)	4057.4	5456.4	0.7436
Gold	(1, 0)	1.2821	1.7099	0.7498
	(1, 1)	919.18	967.25	0.9503
	(2, 0)	557.76	757.83	0.7360
	(2, 1)	2061.2	2436.1	0.8461
Lead	(1, 0)	29.042	29.103	0.9979
	(1, 1)	4932.7	4933.7	0.9998
	(2, 0)	3896.1	3905.1	0.9977
	(2, 1)	12,390	12,400	0.9992

7 Conclusions

By considering small-scale effect on structural and thermal areas via nonlocal continuum theory and dual-phase-lag (DPL) heat conduction model, thermoelastic damping (TED) in thin circular cylindrical nanoshells has been appraised in the paper at hand. Donnell–Mushtari–Vlasov (DMV) equations have also been exploited to model the nanoshell. By choosing time-harmonic asymmetric vibrations of nanoshell, and solving the size-dependent motion, compatibility and heat conduction equations, an analytical relation for evaluation of TED in cylindrical nanoshells with arbitrary boundary conditions has been presented. For the sake of surveying the validity of developed model, a comparison study between the results of current article with those available in the literature has been carried out. To this aim, the nonclassical structural and thermal parameters (i.e. μ, τ_q and τ_T) have been ignored in the provided formulation so that the results of this paper can be compared with those of Lu et al. [14]. In this particular case, the outcomes of the two studies have been in close agreement with each other. In general, the size-dependent results of the current article have been qualitatively similar to the results reported in [14]. For instance, in both papers, irrespective of the elasticity theory and heat conduction model used, thermoelastic damping has been intensified with the increase of dimensions of shell at nanoscales. Additionally, among the four modes examined, in both studies, the most energy dissipation has occurred in modes (1, 1), (2, 1), (2, 0) and (1, 0), respectively. Despite the qualitative similarity of the results, by incorporating scale parameters into calculations, the classical and size-dependent results have been quantitatively different from each other. Accordingly, an in-depth parametric study has been conducted to illuminate the influence of nonlocal parameter, phase lags, vibration modes and type of material on TED in simply supported circular cylindrical nanoshells. The substantial findings of present research can be enumerated as follows:

- By capturing nonlocal effect, the magnitude of TED in circular cylindrical nano-sized shells rises.
- For larger values of nonlocal parameter μ, energy dissipation originated by TED ascends.
- DPL model estimates lower amounts of TED in comparison with CTE model.
- With the increase of dimensions of cylindrical nanoshell, small-scale effect on both structure and heat conduction dwindles and TED value specified via presented size-dependent model in this work tends to that anticipated by means of classical model.
- Depending on the purpose of its usage, the choice of material can be a determining factor in the design of nanoshells. Among the materials appraised in paper at hand, namely copper, gold and lead, cylindrical nanoshells made of lead and gold exhibit the most and least amounts of TED, respectively.

Appendix

The free vibration of a nonlocal Euler–Bernoulli beam is governed by the following equation:

$$EI\frac{\partial^4 w}{\partial x^4} - \mu\rho A\frac{\partial^4 w}{\partial x^2 \partial t^2} + \rho A\frac{\partial^2 w}{\partial t^2} = 0, \tag{59}$$

in which I and A represent the area moment of inertia of cross sections and cross section area of the beam. By adopting simple harmonic form $w(x,t) = \sum_{m=1}^{\infty} W_m(x)e^{i\omega_m t}$, substituting it into equation above, and simplifying the result, one can get:

$$\frac{\partial^4 W_m}{\partial x^4} + \mu\lambda_m^4\frac{\partial^4 W_m}{\partial x^2} - \lambda_m^4 W_m = 0, \tag{60}$$

where

$$\lambda_m^4 = \frac{\rho A}{EI}\omega_m^2. \tag{61}$$

The general solution of Eq. (60) has the following form:

$$W_m = C_1\sin(\gamma_1 x) + C_2\cos(\gamma_1 x) + C_3\sinh(\gamma_2 x) + C_4\cosh(\gamma_2 x), \tag{62}$$

in which C_1, C_2, C_3 and C_4 are integration constants. Substitution of relation above into Eq. (60) and solving the obtained equation gives:

$$\gamma_1^2 = \frac{1}{2}\left(\mu\lambda_m^4 + \sqrt{\mu^2\lambda_m^8 + 4\lambda_m^4}\right) \quad \text{and}$$
$$\gamma_2^2 = \frac{1}{2}\left(-\mu\lambda_m^4 + \sqrt{\mu^2\lambda_m^8 + 4\lambda_m^4}\right). \tag{63}$$

Boundary conditions of three common types of beams, namely doubly simply supported (SS), doubly clamped (CC) and cantilever (CF) are expressed by [38]:

$$SS: \quad W_m(0) = \frac{\mathrm{d}^2 W_m}{\mathrm{d}x^2}(0) = W_m(L) = \frac{\mathrm{d}^2 W_m}{\mathrm{d}x^2}(L) = 0, \tag{64}$$

$$CC: \quad W_m(0) = \frac{\mathrm{d}W_m}{\mathrm{d}x}(0) = W_m(L) = \frac{\mathrm{d}W_m}{\mathrm{d}x}(L) = 0, \tag{65}$$

$$CF: \quad W_m(0) = \frac{\mathrm{d}W_m}{\mathrm{d}x}(0) = EI\frac{\mathrm{d}^2 W_m}{\mathrm{d}x^2}(L) + \mu\rho A\omega_m^2 W_m(L) = EI\frac{\mathrm{d}^3 W_m}{\mathrm{d}x^3}(L) + \mu\rho A\omega_m^2\frac{\mathrm{d}W_m}{\mathrm{d}x}(L) = 0. \tag{66}$$

By inserting Eq. (62) into Eqs. (64)–(66), using Eq. (61) and setting the determinant of the coefficient matrix of the obtained algebraic equations for C_1, C_2, C_3 and C_4 to zero, one can attain the following characteristic equations:

$$SS: \quad \sin(\gamma_1 L) = 0, \tag{67}$$

$$CC: \quad 2\cos(\gamma_1 L)\cosh(\gamma_2 L) + \left(\frac{\gamma_1}{\gamma_2} - \frac{\gamma_2}{\gamma_1}\right)\sin(\gamma_1 L)\sinh(\gamma_2 L) - 2 = 0, \tag{68}$$

$$CF: \quad 2\cos(\gamma_1 L)\cosh(\gamma_2 L) + \left(\frac{\gamma_1}{\gamma_2} - \frac{\gamma_2}{\gamma_1}\right)\sin(\gamma_1 L)\sinh(\gamma_2 L) + \left(\frac{\gamma_1^2}{\gamma_2^2} + \frac{\gamma_2^2}{\gamma_1^2}\right) = 0. \tag{69}$$

By considering the relation of γ_1 and γ_2 with λ_m through relation (63) and solving the equations above, γ_1 and γ_2 are extracted, and by inserting them in Eq. (62), the mode shape of nonlocal beams with mentioned boundary conditions is obtained. Since the model of Lu et al. [14] has been provided in the context of classical continuum theory (i.e. $\mu = 0$) for CC boundary conditions, according to Eq. (63), the comparison study must be conducted on the basis of $\gamma_1 = \gamma_2 = \lambda_m$. Hence, by considering Eq. (68), the characteristic equation of a classical CC beam becomes:

$$\cos(\lambda_m L)\cosh(\lambda_m L) - 1 = 0 \tag{70}$$

On the other hand, by imposing boundary conditions (65) on Eq. (62) and letting $\gamma_1 = \gamma_2 = \lambda_m$, the mode shape of a classical CC beam is obtained as follows:

$$W_m = C_1\left[(\sin(\lambda_m x) - \sinh(\lambda_m x)) - \frac{\sin(\lambda_m L) - \sinh(\lambda_m L)}{\cos(\lambda_m L) - \cosh(\lambda_m L)}(\cos(\lambda_m x) - \cosh(\lambda_m x))\right]. \tag{71}$$

Acknowledgements The study was supported by Heilongjiang Provincial Natural Science Foundation of China (LC2017028), Basic Scientific Research Business Expense Research Project of Heilongjiang Provincial Colleges and Universities (135409102), and Academic Backbone Project of Heilongjiang Provincial Department of Education (135509413).

Declarations

Conflict of interest The authors declare that they have no conflict of interest.

Ethical approval This article does not contain any studies with human participants or animals performed by any of the authors.

References

1. Fleck NA, Muller GM, Ashby MF, Hutchinson JW. Strain gradient plasticity: theory and experiment. Acta Metall Mater. 1994;42(2):475–87.
2. Ma Q, Clarke DR. Size dependent hardness of silver single crystals. J Mater Res. 1995;10(4):853–63.
3. McFarland AW, Colton JS. Role of material microstructure in plate stiffness with relevance to microcantilever sensors. J Micromech Microeng. 2005;15(5):1060.
4. Toupin RA. Theories of elasticity with couple-stress. Arch Ration Mech Anal. 1964;17(2):85–112.

5. Eringen AC. Linear theory of nonlocal elasticity and dispersion of plane waves. Int J Eng Sci. 1972;10(5):425–35.
6. Yang FACM, Chong ACM, Lam DCC, Tong P. Couple stress based strain gradient theory for elasticity. Int J Solids Struct. 2002;39(10):2731–43.
7. Lam DC, Yang F, Chong ACM, Wang J, Tong P. Experiments and theory in strain gradient elasticity. J Mech Phys Solids. 2003;51(8):1477–508.
8. Xu M, Li X. The modeling of nanoscale heat conduction by Boltzmann transport equation. Int J Heat Mass Transf. 2012;55(7–8):1905–10.
9. Lord HW, Shulman Y. A generalized dynamical theory of thermoelasticity. J Mech Phys Solids. 1967;15(5):299–309.
10. Tzou DY. Macro-to microscale heat transfer: the lagging behavior. John Wiley & Sons; 2014.
11. Guyer RA, Krumhansl JA. Solution of the linearized phonon Boltzmann equation. Phys Rev. 1966;148(2):766.
12. Zener C. Internal friction in solids I Theory of internal friction in reeds. Phys Rev. 1937;52(3):230.
13. Lifshitz R, Roukes ML. Thermoelastic damping in micro-and nanomechanical systems. Phys Rev B. 2000;61(8):5600.
14. Lu P, Lee HP, Lu C, Chen HB. Thermoelastic damping in cylindrical shells with application to tubular oscillator structures. Int J Mech Sci. 2008;50(3):501–12.
15. Kim SB, Kim JH. Quality factors for the nano-mechanical tubes with thermoelastic damping and initial stress. J Sound Vib. 2011;330(7):1393–402.
16. Li P, Fang Y, Hu R. Thermoelastic damping in rectangular and circular microplate resonators. J Sound Vib. 2012;331(3):721–33.
17. Yue X, Yue X, Borjalilou V. Generalized thermoelasticity model of nonlocal strain gradient Timoshenko nanobeams. Arch Civil Mech Eng. 2021;21(3):1–20.
18. Xiao C, Zhang G, Hu P, Yu Y, Mo Y, Borjalilou V. Size-dependent generalized thermoelasticity model for thermoelastic damping in circular nanoplates. Waves Random Complex Media 2021; 1–21.
19. Li F, Esmaeili S. On thermoelastic damping in axisymmetric vibrations of circular nanoplates: incorporation of size effect into structural and thermal areas. Eur Phys J Plus. 2021;136(2):1–17.
20. Zhong ZY, Zhang WM, Meng G, Wang MY. Thermoelastic damping in the size-dependent microplate resonators based on modified couple stress theory. J Microelectromech Syst. 2014;24(2):431–45.
21. Zhang H, Kim T, Choi G, Cho HH. Thermoelastic damping in micro-and nanomechanical beam resonators considering size effects. Int J Heat Mass Transf. 2016;103:783–90.
22. Zhang C, Wang L, Eyvazian A, Khan A, Sebaey TA, Farouk N. Analytical study of the damping vibration behavior of the metal foam nanocomposite plates reinforced with graphene oxide powders in thermal environments. Arch Civil Mech Eng. 2021;21(4):1–23.
23. Parayil DV, Kulkarni SS, Pawaskar DN. A generalized model for thermoelastic damping in beams with mid-plane stretching nonlinearity. Int J Mech Sci. 2018;135:582–95.
24. Deng W, Li L, Hu Y, Wang X, Li X. Thermoelastic damping of graphene nanobeams by considering the size effects of nanostructure and heat conduction. J Therm Stress. 2018;41(9):1182–200.
25. Rashahmadi S, Meguid SA. Modeling size-dependent thermoelastic energy dissipation of graphene nanoresonators using nonlocal elasticity theory. Acta Mech. 2019;230(3):771–85.
26. Li SR, Ma HK. Analysis of free vibration of functionally graded material micro-plates with thermoelastic damping. Arch Appl Mech. 2020;90:1285–304.
27. Kumar H, Mukhopadhyay S. Thermoelastic damping analysis for size-dependent microplate resonators utilizing the modified couple stress theory and the three-phase-lag heat conduction model. Int J Heat Mass Transf. 2020;148:118997.
28. Yang Z, Cheng D, Cong G, Jin D, Borjalilou V. Dual-phase-lag thermoelastic damping in nonlocal rectangular nanoplates. Waves Random Complex Media 2021;1–20.
29. Ahmadi HR, Rahimi Z, Sumelka W. Thermoelastic damping in orthotropic and isotropic NEMS resonators accounting for double nonlocal thermoelastic effects. J Therm Stress. 2020;44(3):342–58.
30. Shi S, He T, Jin F. Thermoelastic damping analysis of size-dependent nano-resonators considering dual-phase-lag heat conduction model and surface effect. Int J Heat Mass Transf. 2021;170:120977.
31. Zhou H, Li P. Nonlocal dual-phase-lagging thermoelastic damping in rectangular and circular micro/nanoplate resonators. Appl Math Model. 2021;95:667–87.
32. Ge X, Li P, Fang Y, Yang L. Thermoelastic damping in rectangular microplate/nanoplate resonators based on modified nonlocal strain gradient theory and nonlocal heat conductive law. J Therm Stress. 2021;44(6):1–30.
33. Weng W, Lu Y, Borjalilou V. Size-dependent thermoelastic vibrations of Timoshenko nanobeams by taking into account dual-phase-lagging effect. Eur Phys J Plus. 2021;136(7):1–26.
34. Zhou H, Li P. Dual-phase-lagging thermoelastic damping and frequency shift of micro/nano-ring resonators with rectangular cross-section. Thin Wall Struct. 2021;159:107309.
35. Arshid E, Arshid H, Amir S, Mousavi SB. Free vibration and buckling analyses of FG porous sandwich curved microbeams in thermal environment under magnetic field based on modified couple stress theory. Arch Civil Mech Eng. 2021;21(1):1–23.
36. Soedel W, Qatu MS. Vibrations of shells and plates. New York: Dekker; 2005.
37. Borjalilou V, Asghari M. Thermoelastic damping in strain gradient microplates according to a generalized theory of thermoelasticity. J Therm Stress. 2020;43(4):401–20.
38. Borjalilou V, Asghari M, Taati E. Thermoelastic damping in nonlocal nanobeams considering dual-phase-lagging effect. J Vib Control. 2020;26(11–12):1042–53.